Applied Energy 355 (2024) 122253

Contents lists available at ScienceDirect

Applied Energy

journal homepage: www.elsevier.com/locate/apenergy

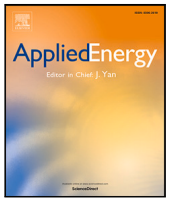

A low-frequency ferrohydrodynamic pump for a magneto-caloric refrigerator

Keerthivasan Rajamani [a,*], Eva Juffermans [a], Luca Granelli [a], Ana De Cuadra Rabaneda [a], Wilko Rohlfs [a], Marcel ter Brake [b], Theo van der Meer [a], Mina Shahi [a]

[a] Department of Thermal and Fluid Engineering, Faculty of Engineering Technology, University of Twente, Enschede, The Netherlands
[b] Energy Materials and Systems, Faculty of Science and Technology, University of Twente, Enschede, The Netherlands

ARTICLE INFO

Keywords:
Ferrofluid
Ferrohydrodynamics
Magnetic pumping
Magnetocaloric refrigerator
EFH1
No moving parts

ABSTRACT

Ferrohydrodynamic or magnetic pumping enables the design of a magnetocaloric refrigerator with no moving parts. Existing magnetic pumps utilize travelling wave magnetic fields with frequencies in the range of 100 to 1000 Hz. Such high frequencies when utilized in the proposed refrigerator could cause heating which is detrimental to its performance. Hence, a magnetic pump that works with low magnetic field frequencies (< 1 Hz) is designed and its performance is experimentally characterized and compared against an one-dimensional model. The design of the magnetic pump consists of a rising and falling pipe, circumscribed by an electromagnetic coil. On application of a magnetic field, due to the inward acting force on either end of the pipes, the ferrofluid progresses in the rising pipe and reaches the falling pipe. On removal of the magnetic field, the portion of the fluid in the falling pipe falls down due to gravity, thereby achieving a net pumping action. Thus on continuously cycling the magnetic field, an intermittent motion of the ferrofluid is obtained. The maximum cross-sectional area and time-averaged mass flow rate of the proposed design is 1.8 g s^{-1} cm^{-2} at 0.74 Hz and 35.7 mT. This mass flow rate is comparable to pump designs that work on travelling wave magnetic fields, whose operational frequency is three orders of magnitude higher.

1. Introduction

The dominant technology used for refrigeration is the Vapour Compression Refrigeration System [1]. In this, the temperature change is obtained through a cyclic process of compression and expansion of a refrigerant fluid. This process adds a considerable source of irreversibility to the system. Among the many alternatives, magnetic refrigeration is a promising technology [2]. It can be up to 20% more energy efficient than a conventional refrigeration system [3,4]. Furthermore, due to the absence of harmful, ozone-depleting chemicals, and greenhouse gases, magnetic refrigeration is considered to be environmentally friendly [5].

When a magnetocaloric material in an adiabatic condition is subjected to varying magnetic fields, it undergoes a temperature change [6]. This effect was discovered by Weiss and Picard in 1917 [7,8]. They observed nickel being reversibly heated during magnetization near its Curie temperature, and noted that the reversible nature of heating distinguishes itself from heating due to hysteresis [7,8]. The magnetocaloric effect is due to the reduction in the magnetic entropy of the material, which leads to an increase in lattice entropy, as the overall entropy of the system is constant in an adiabatic process [9]. When the excess heat is transferred to the ambient, and followed by an adiabatic demagnetization, the magnetocaloric material experiences a reduction in its temperature. This reduction happens due to the increase in the magnetic entropy at the expense of a reduction in lattice entropy. This temperature change is used to obtain refrigeration in a magnetic refrigerator [4,10–12].

The magnetocaloric effect was initially applied in cryogenics where the temperature drop obtained during adiabatic demagnetization of paramagnetic salts was utilized to reach temperatures close to absolute zero [13–15]. Room temperature application was initiated by Brown in 1976, when he built an experimental system utilizing gadolinium [16] and a regenerator fluid that achieved no-load temperature extremes of 272 K and 319 K. The subsequent prototypes from the research community explored further designs, for example, different material compositions, rotary and linear movement between the magnetocaloric material and the magnetic field source, and regenerators to increase the temperature span [2,17–19]. In all the experimentally built magnetic refrigerator so far, a porous/plate form of the magnetocaloric material is used through which a heat transfer liquid passes [20]. Such systems use a mechanical actuator/pump and valves for liquid circulation and control. While they serve their purpose, the former leads to reliability issues due to moving parts while the latter leads to considerable pressure drop affecting system performance.

* Corresponding author.
E-mail address: k.rajamani@utwente.nl (K. Rajamani).

https://doi.org/10.1016/j.apenergy.2023.122253
Received 21 June 2023; Received in revised form 3 October 2023; Accepted 1 November 2023
Available online 9 November 2023

To address the above-mentioned issues, a mixture of magnetocaloric material and heat transfer liquid can be used in a system as shown in Fig. 1. It consists of a stationary magnet assembly surrounding the hot heat exchanger, magnetic pump, and cold heat exchanger. Since the mixture is magnetic, it offers the possibility to circulate the mixture using magnetic fields, thereby resulting in a magnetic refrigerator with no moving parts. As the mixture enters the region of the magnet assembly, the magnetocaloric material experiences an increase in temperature due to the magnetocaloric effect. It is simultaneously transferred to the heat transfer liquid until they are in thermal equilibrium in the mixture. The mixture now exchanges heat with the ambient through the hot heat exchanger. The mixture then exits the hot heat exchanger, where it is demagnetized and therefore experiences a temperature reduction. It is circulated by the magnetic pump to the cold heat exchanger, where it absorbs heat from the system to be refrigerated. It then enters the hot heat exchanger completing a cycle.

The interactions between the forces of a magnetic body and the magnetic fields can be used to impart motion to the former. A magnetic particle exposed to a magnetic field gradient tends to move towards an area with a higher magnetic field. When such particles, e.g. nanometre-sized magnetite (Fe_3O_4), are suspended in a carrier fluid such as water or oil, magnetic fluids or ferrofluids are formed [21,22]. Ferrofluids are used in a wide range of applications, from cancer therapy to loudspeakers [23–27].

By utilizing the magnetic body force, also known as the Kelvin force, ferrofluids can be set in motion by spatial or temporal variation of the magnetic fields. With suitable flow geometry, magnetic or ferrohydrodynamic pumping can be achieved. This is different from magnetohydrodynamic and electrohydrodynamic pumping. Magnetohydrodynamic pumping uses the force experienced by an electrically charged particle in a magnetic field (Lorentz force), while electrohydrodynamic pumping uses the force experienced by electrically charged particles in electric fields [21,28,29].

Magnetic or ferrohydrodynamic pumping involves either pumping the ferrofluid itself or using the ferrofluid to pump a non-magnetic fluid that is immiscible with the ferrofluid. In either case, the result is a pump with no moving parts, which is one of the main advantages of ferrohydrodynamic pumping, resulting in longer life, higher reliability and compactness. In addition, vibration is significantly reduced, resulting in quiet operation. Ferrohydrodynamic pumps can also be used in areas where direct contact between the liquid and the pump is not desired. In this case, a mechanical peristaltic pump is an alternative, but it usually generates significant shear stress in the liquid during the pumping process. This is undesirable in certain cases, such as pumping human blood, where excessive shear stress can damage cells. Even in such cases, ferrofluid can be used to create a hollow core into which blood can be pumped with less damage [30].

When ferrofluid is used to pump an immiscible fluid, this is normally done through one or more ferrofluid plugs, with the immiscible fluid occupying the space between the ferrofluid plugs. The movement of the magnetic field moves the ferrofluid plugs, pumping the non-magnetic fluid [31,32]. Magnetic polymers/elastomers are used to make a magnetic tube whose deformation under alternating magnetic fields is used to pump a non-magnetic fluid [33–35]. Such magnetic peristaltic pumps are also used in lab-on-chip systems [36].

When ferrofluid is the fluid to be moved, this is achieved by a spatial or a combination of spatial and temporal variation of the magnetic field. In cases where there is only a spatial variation in the magnetic field, pumping is achieved by heating the ferrofluid in the vicinity of the magnet. In the presence of a temperature gradient, the temperature dependence of the magnetization of the ferrofluid is used to attract the colder fluid, while the hotter fluid is displaced from the region of the applied magnetic field. This is the principle of thermomagnetic convection [37], and one of the early works [38] reported its use in magnetocaloric energy conversion devices for waste heat utilization, where the work required for pumping is provided by the heat source. It can be used to build cooling devices that require no external power [39].

In the absence of a temperature gradient, it is possible to pump a ferrofluid by a combination of spatial and temporal variation of the magnetic field. One of the first studies to use magnetic body force to induce motion in a ferrofluid was carried out by Moskowitz and Rosensweig [40]. They exposed a ferrofluid in a cylindrical container to a uniform magnetic field rotating at different angular velocities. Their ferrofluid consisted of polydisperse suspensions, with those suspensions that did not exhibit superparamagnetic behaviour physically rotating with the external magnetic field due to the magnetic torque. This caused viscous drag with the surrounding fluid, resulting in macroscopic rotation of the fluid. The rate of macroscopic fluid rotation was found to be linearly dependent on the applied field strength, while a non-linear dependence on the field frequency was observed. In a preliminary study without optimization of the parameters involved, macroscopic fluid rotation rates of $\approx$ 60 and 160 rpm were obtained at 100 Hz and 1000 Hz, respectively with a field strength of 4.3 mT.

Prior work in the literature has dealt with the theoretical analysis of a planar ferrofluid layer subjected to a travelling wave current sheet [41] and a system with a non-uniform travelling wave magnetic field [42,43]. The ferrohydrodynamic pumping of a magnetic fluid caused by spatially travelling and sinusoidally time-varying magnetic fields in a planar channel was numerically investigated and it was found that, due to the nature of the magnetic field variation, both magnetic body force and magnetic torque contribute to the pumping [44]. Magnetic field frequencies up to 1 MHz have been studied. It was found that the period of the travelling wave has a strong influence on the flow velocity. The maximum flow velocity averaged over the cross section was obtained when the product of the channel height and the wave number was close to 1 and also when the magnetic field frequency was the reciprocal of the relaxation time constant (in their case 10 μs) for the magnetic fluid.

An experimental investigation of ferrohydrodynamic pumping using the above magnetic field configuration (spatially travelling and sinusoidally time-varying) in a circular channel was conducted by Mao et al. [45]. The channel formed a rectangular closed loop and it was fully filled with a commercial ferrofluid — EFH1 (Ferrotec Corporation). The flow velocity was found to be dependent on both the excitation current (varied from 5 A to 12 A) and the frequency (100 Hz to 2 kHz). The optimal frequency of pumping was in the range of 500 Hz to 1000 Hz for the values of the current studied. A maximum flow velocity of 7.4 $mm\,s^{-1}$ was achieved (pipe internal diameter = 15.4 mm) at 12 A and 1000 Hz. The critical particle diameter for the transition from Néel to Brownian relaxation mechanism was 15.2 nm, while most ($\approx$ 96%) of the particles had a core diameter of less than 12.1 nm. Due to the dominance of the Néel relaxation mechanism (in which there would be no physical rotation of particles), individual particles by themselves cannot have caused the observed flow. So they conjecture that the individual particles reversibly form dimers (model discussed in [46]) even in the presence of moderate magnetic fields ($\approx$10 mT used in their study). These dimers rotate due to the magnetic field configuration, thus contributing to the observed flow.

The existing research in ferrohydrodynamic pumping without any mechanically moving parts utilizes magnetic field frequencies in the range of 100 Hz to 1000 Hz. This frequency range usually has no adverse effects on their intended areas of application. However, for usage in a magnetocaloric mixture based refrigerator (Fig. 1), the frequency is limited by the following factors: (i) physical rotation of magnetocaloric particle chains in high frequencies could lead to heat generation due to viscous dissipation; (ii) for the magneto-caloric mixture, when compared with using water or alcohol as the heat transfer liquid, using room temperature liquid metals will result in higher performance of the refrigerator. However, the use of high-frequency magnetic fields in conjunction with liquid metals would lead to the generation of eddy

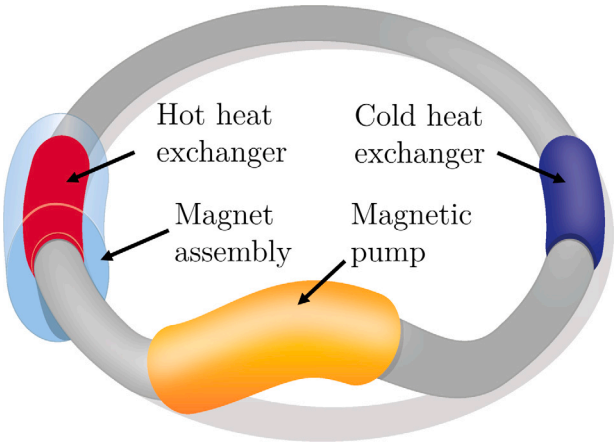

Fig. 1. Illustration of the proposed pump design applied to a magnetic refrigerator. The pump consists of a rising and a falling pipe enclosed by an electromagnetic coil, and its working is shown in Fig. 2.

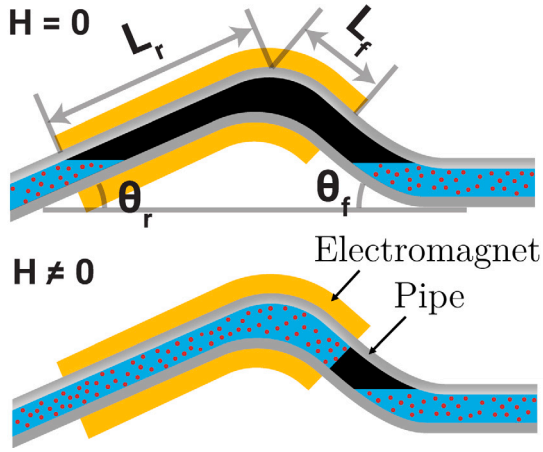

Fig. 2. Illustration of the ferrofluid position when the electromagnet is powered off ($H = 0$) and when it is powered on ($H \neq 0$).

currents and thus to the heating of the mixture. This would have a detrimental effect on the performance of the refrigerator system.

Therefore, the current work presents and discusses a ferrohydrodynamic pump that operates at low frequencies (around 1 Hz) while achieving similar mass fow rates to pumps operating at two to three orders of magnitude higher frequencies. Unlike existing work that uses magnetic rotational force (or torque), the novelty of the developed pump is that it uses magnetic translational force in combination with inclined pipes to achieve the pumping action. In addition, previous works typically uses multi-channel phase-shifted alternating current to achieve the motion, while the current pump uses a single-channel pulsed direct current. This simplifies the electrical hardware requirements thereby reducing the overall complexity of the system. The low-frequency pump developed can be used in a magnetocaloric mixture-based refrigerator (and other applications) where heating effects from high-frequency magnetic fields are not desired.

2. Methodology

The proposed pump design applied to a magnetocaloric mixture based refrigerator is shown in Fig. 1, and its working is shown in Fig. 2. It consists of a rising and a falling pipe that is enclosed by an electromagnetic coil. When the electromagnet is powered off, the resting level of the ferrofluid is shown in Fig. 2 (top). When the electromagnet is powered on, the ferrofluid near the rising pipe will experience a magnetic force, as explained in next section, that causes it to rise and reach the falling pipe. As it reaches the end of the electromagnet in the falling pipe, it will experience an inward acting force, due to which it no longer moves, and attains an equilibrium position as shown in Fig. 2 (bottom). When the electromagnet is powered off, the ferrofluid in the rising and falling pipe will fall on their respective sides due to the gravitational force. Thus a net pumping is obtained by a combination of magnetic and gravitational forces. In certain scenarios, gravitational force may not be present. An example is in thermal management for space applications, where system reliability is important. In such cases, the developed pump can be modified to have an intermediate energy storage medium such as a compressed bubble for its operation.

Table 1
Properties of EFH1 ferrofluid. Density and viscosity are measured, while other property values are taken from EFH data sheet [47].

Property	Value	Units
Density (at 17 °C)	$1180 \pm 1.5\%$	$\mathrm{kg\,m^{-3}}$
Dynamic viscosity (at 17 °C)	$9.1 \times 10^{-3} \pm 4\%$	$\mathrm{kg\,m^{-1}\,s^{-1}}$
Flash point	95	°C
Boiling point	223	°C
Auto-ignition temperature	215	°C
Carrier liquid	Hydrocarbon oil	
Suspension	Fe_3O_4 nanoparticles	

For design and analysis of the proposed pump, EFH1, a commercial ferrofluid from Ferrotec Corporation is used as a test liquid. It is widely used in the scientific literature and therefore allows for meaningful comparison with other studies, for example with [46]. The properties of EFH1 are given in the Table 1. The operating temperature of 17 °C is well below the flash and boiling point of the ferrofluid for safe operation.

2.1. Magnetic force

When a magnetic particle is exposed to a spatial gradient in the magnetic field, it experiences a magnetic body force, also known as Kelvin force, given by Eq. (1). The direction of this force is towards increasing magnetic field intensity.

$$\boldsymbol{F}_{\mathrm{MBF}} = \mu_0 \left(\bar{\boldsymbol{M}} \cdot \boldsymbol{\nabla}\right) \boldsymbol{H} \tag{1}$$

where F_{MBF} is the magnetic body force per unit volume [$\mathrm{N\,m^{-3}}$], μ_0 is the magnetic permeability of vacuum [$\mathrm{kg\,m\,s^{-2}\,A^{-2}}$], $\bar{M}$ is the magnetization of the particle [$\mathrm{A\,m^{-1}}$], and H is the applied magnetic field [$\mathrm{A\,m^{-1}}$]. Note that the units of $\mu_0 H$ is represented by tesla, T.

The magnetization of a ferrofluid is a function of both the applied magnetic field and its temperature, $\bar{M}(H,T)$. However, in the present work the temperature of the ferrofluid during experiments remained nearly at a constant value of 17.0 ± 1.0 °C. In this context, the magnetization depends only on the applied magnetic field, $\bar{M}(H)$. Isothermal magnetization measurements were performed in the Vibrating Sample Magnetometer option of the Physical Property Measurement System (Quantum Design Inc.). The resulting magnetization curve of the ferrofluid is shown in Fig. 3 for 17.0 °C.

3. Experimental setup

In order to understand the dynamics of the magnetic pumping process that involves inclined pipes (Fig. 2), we proceed by first analysing the dynamics of a ferrofluid height rise in a vertical pipe. The schematic and actual view of the experimental setup used to study this is shown in Fig. 4. It consists of a reservoir (inner diameter = 150 mm) that is connected to the vertical pipe (material — PMMA, inner diameter = 6 mm, outer diameter = 10 mm) through a series of two connecting pipes. A tightly wound electromagnetic coil (inner diameter = 10 mm,

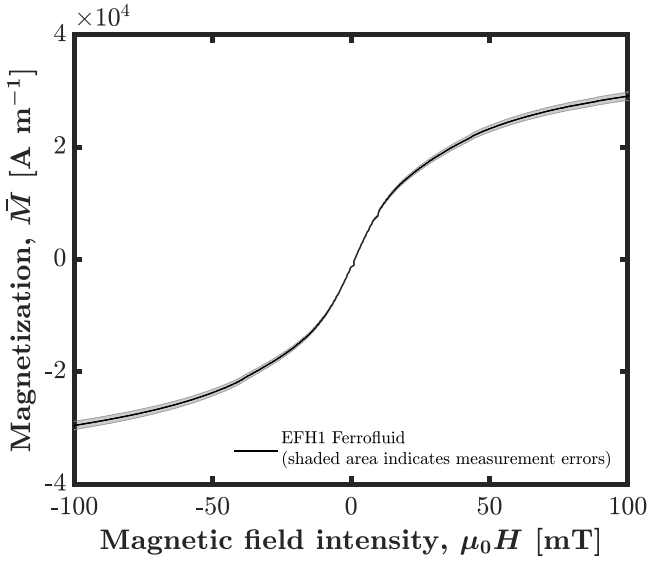

Fig. 3. Variation in magnetization of the ferrofluid used for experiments with applied magnetic field at 17.0 °C.

outer diameter = 22 mm) with 3 layers using 2 mm insulated copper wire is wrapped around the vertical pipe. The electromagnet length (170 mm) is chosen to be long enough such that the steady-state height reached by the ferrofluid, for the tested magnetic field strengths, near one end of the electromagnet will not experience the opposing force caused by the other end of the electromagnet. The change in height of the ferrofluid in the reservoir, and thereby in the vertical pipe, was measured by a confocal laser displacement sensor (CL-L030, Keyence Corporation). The data collection rate was 1000 Hz. For magnetic pumping experiments, the vertical pipe in Fig. 4 is replaced with an inclined rising and falling pipe (Fig. 2, Fig. 10). The end of the falling pipe is open to the atmosphere, and the pumped mass of the ferrofluid is measured by collecting it over a mass balance (BCE323i-1s, Sartorius GmbH). The electromagnet was powered with a direct-current power supply (TTi TSX1820, TEquipment Interworld Highway, LLC). For magnetic pumping, powering the electromagnet on/off was obtained by integrating a solid state relay (Crydom D1D40) activated by a function generator (HP 33120 A).

3.1. Magnetic field

The magnetic field caused by the electromagnetic coil in the pipe is three-dimensional. Since only its axial component is relevant for ferrofluid height rise, the other two components, which are also relatively lower in magnitude, are neglected. The axial magnetic field along the pipe axis for different current amplitudes supplied to the electromagnet is shown in Fig. 5. Here, 0 mm in the axial position corresponds to the bottom end of the electromagnetic coil.

As would be expected, the magnetic field exhibits a gradual increase in its magnitude before the start of the electromagnetic coil (Fig. 5), followed by a region of steep increase. Ideally, it should then approach an uniform value. However, the aberrations in the magnetic field observed in Fig. 5 are likely due to imperfections in the coil winding among the different layers.

The length of the electromagnet (170 mm) is long when compared to the maximum height rise observed in the experiments (<50 mm). This implies that the ferrofluid would only experience the force due to the bottom half of the electromagnet. Therefore, magnetic field measurements are shown only till 60 mm in Fig. 5. These measurements were taken by positioning the tesla meter probe (FM 302, Projekt Elektronik GmbH) concentrically with the electromagnetic coil. The movement of the probe was obtained by a motorized positioning system (OWIS GmbH). The probe had an outer diameter of 6 mm and a length of 80 mm, with one of its ends connected to the data acquisition box. The probe had a field measurement sensor mounted on its axis at the free end with a cross-sectional area of 1 mm × 1 mm. Thus the probe measured the magnetic field along the central axis of the electromagnetic coil. The measurements were repeated by positioning the probe at various parallel lines located within ± 2 mm from the central axis of the electromagnetic coil. The deviation in the magnetic field measurements observed between them was less than 2%. Therefore, the measurement along the central axis of the electromagnetic coil is assumed to be uniform across the cross-section at a given axial position. It follows that the magnetic field caused by the electromagnet for a given current depends only on the axial position in the pipe, i.e. $H(h)$.

3.2. Dynamics of ferrofluid rise in pipe

To understand the dynamics of the ferrofluid rise when the magnetic field is powered on, the one-dimensional form of Newton's second law of motion is applied to the ferrofluid as given by Eq. (2). Here, the left side represents the net external force acting on the ferrofluid which is given by the summation of the total magnetic force F_M acting on the ferrofluid causing it to rise, and negative of gravitational F_g, and frictional F_f forces that act against the ferrofluid rise. For a given geometry and fluid properties, these forces are time-dependent. The summation of the four terms at the right side of Eq. (2) represents the time rate of momentum change of the ferrofluid in the reservoir, two connecting sections, and in the vertical pipe, respectively. Of these 4 terms, as the ferrofluid is fully filled in the connecting sections, velocity is the only parameter that is variable in the second and third terms for a given geometry. As the ferrofluid mass changes in the vertical pipe and the reservoir, the first and fourth term has height and velocity as variables.

$$F_M(t) - F_g(t) - F_f(t) = \frac{d}{dt}\left[\left[\rho A_r h_r(t)\frac{dh_r(t)}{dt}\right] + \left[\rho A_{c1} l_{c1} v_{c1}(t)\right] + \left[\rho A_{c2} l_{c2} v_{c2}(t)\right] + \left[\rho A_p h_p(t)\frac{dh_p(t)}{dt}\right]\right] \quad (2)$$

where ρ is the density of the ferrofluid [kg m^{-3}], A is the cross-sectional area [m^2], h is the ferrofluid height [m], l is the length of the connecting section [m], and v is the velocity of the ferrofluid [m s^{-1}]. The subscripts r, c1, c2, and p refer to the reservoir, connecting sections 1, 2, and pipe respectively.

The total magnetic force, $F_M(t)$, acting on the ferrofluid is obtained by integration of Eq. (1) in its one-dimensional form over the relevant volume of the ferrofluid, as given by Eq. (3).

$$F_M(t) = \mu_0 A_p \int_{h=h_A}^{h=h_I+h_p(t)} \bar{M}(H)\frac{dH(h)}{dh}dh \quad (3)$$

where the reference point h_A is defined at a position sufficiently far below the electromagnetic coil such that the magnetic field is zero when the electromagnet is powered on. The initial level ($t = 0$) of the ferrofluid, i.e. before the electromagnet is powered on, is represented by h_I, which is measured relative to h_A. The time-dependent ferrofluid height in the pipe $h_p(t)$ is measured relative to the initial ferrofluid level in the reservoir $h_r(t = 0)$. Note that the applied magnetic field H depends on the electromagnetic coil design and the current passed through it.

The gravitational force acting on the rising ferrofluid is given by Eq. (4).

$$F_g(t) = \rho\ A_p\ g\ h_p(t)\ (sin\ \theta + \alpha), \quad \alpha = \frac{A_p}{A_r} \quad (4)$$

where g is the acceleration due to gravity [m s^{-2}], and θ is the inclination angle of the pipe with respect to the horizontal ($\theta = 90°$ for a

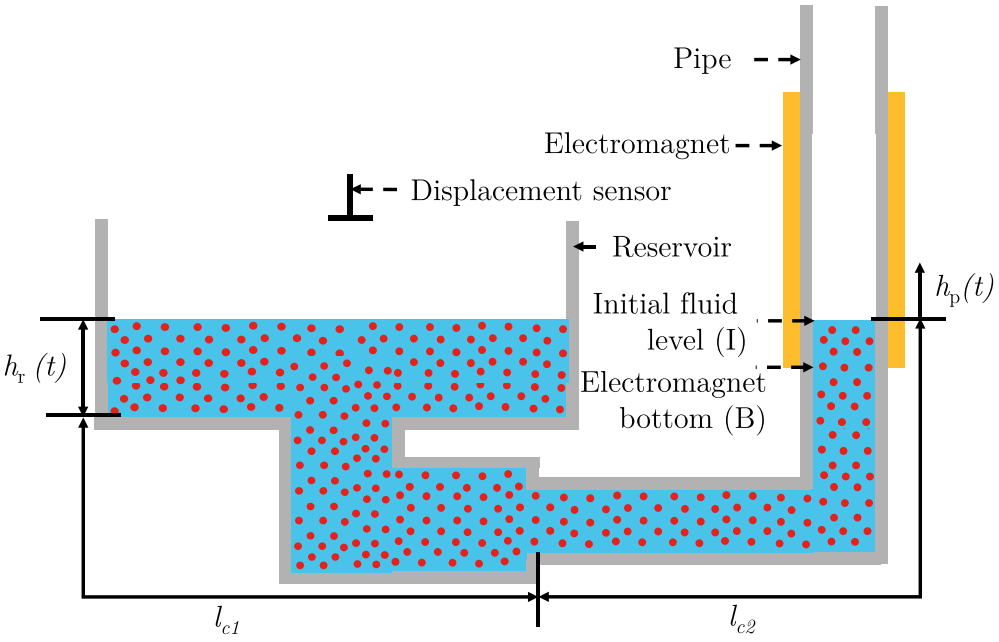

(a)

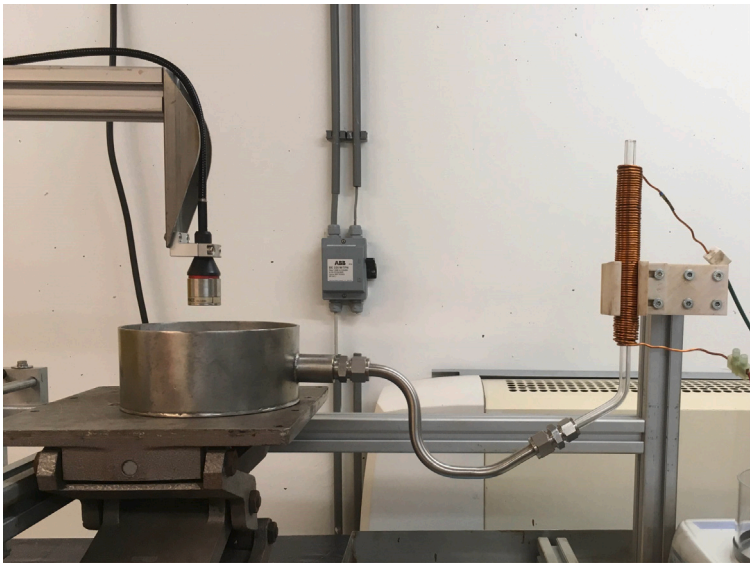

(b)

Fig. 4. (a) Experimental setup illustration for vertical height rise measurements. (b) View of the actual setup.

vertical pipe). Note that $h_p(t)$ measures the height relative to initial ferrofluid level in the reservoir $h_r(t = 0)$. As the ferrofluid rises in the pipe, due to mass conservation, its level lowers in the reservoir. So the gravitational force acting on the ferrofluid (Eq. (4)) should account for the total vertical ferrofluid height in the pipe which is $h_p(t)sin\ \theta + h_{r\text{-}c}(t)$. Here $h_{r\text{-}c}(t)$ is the reduction in the ferrofluid height at the reservoir when compared to $h_r(t = 0)$. Since ferrofluid's density remains unchanged, mass conservation yields $h_{r\text{-}c}(t) = \alpha h_p(t)$, and it is accordingly accounted for in Eq. (4).

For all the experiments of ferrofluid rise, its Reynolds number was well below 2000. So the flow is considered to be laminar. The pressure drop experienced by the ferrofluid is assumed to be given by Hagen–Poiseuille law. So the frictional force experienced by the ferrofluid as it flows through the reservoir, two connecting sections, and the pipe is given by Eq. (5).

$$F_f(t) = 8\,\pi\,\mu\,\left[\left[h_r(t)\,\frac{dh_r(t)}{dt}\right] + \left[l_{c1}\ v_{c1}(t)\right] + \left[l_{c2}\ v_{c2}(t)\right] + \left[h_p(t)\,\frac{dh_p(t)}{dt}\right]\right] \tag{5}$$

where μ is the dynamic viscosity [$kg\,m^{-1}\,s^{-1}$] of the ferrofluid used [Table 1].

By the law of conservation of mass, and incompressibility of the ferrofluid considered, the decrease in fluid volume in the reservoir must be equal to the increase in fluid volume in the vertical pipe, and is given by Eq. (6) and (7).

$$h_r(t) = h_r(0) - \alpha\ h_p(t) \tag{6}$$

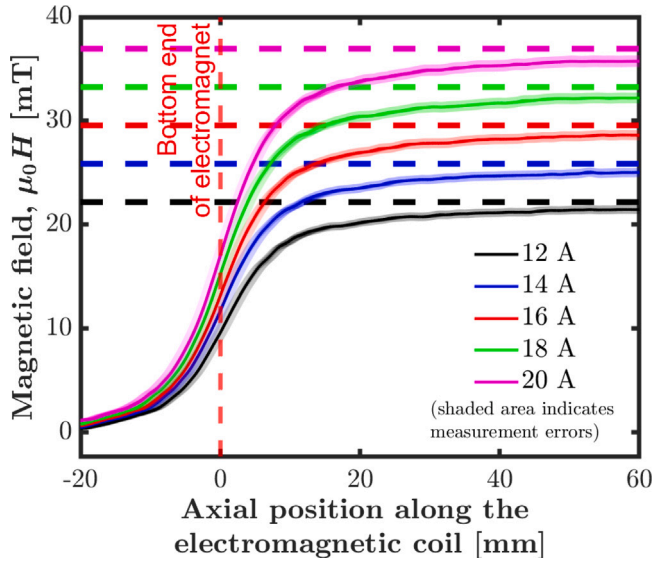

Fig. 5. Measurement of the axial magnetic field along the bottom half length of the electromagnetic coil for different current amplitudes (I). The horizontal dashed lines represents the theortical magnetic field given by $\mu_0 nI$, where n is the number of turns per unit length.

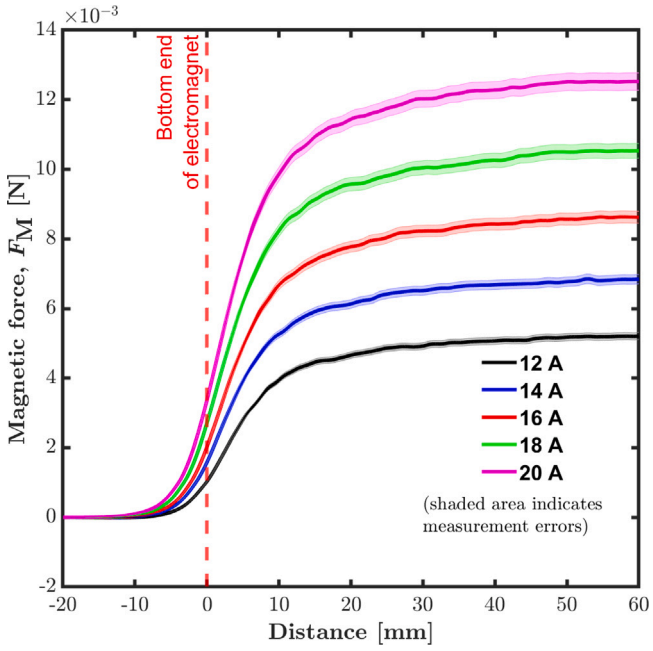

Fig. 6. Magnetic force acting on the ferrofluid as a function of its level in the pipe as given by Eq. (3) for different current amplitudes.

$$\frac{dh_r(t)}{dt} = -\alpha \frac{dh_p(t)}{dt} \tag{7}$$

Similarly, the ferrofluid flow rate through the connecting sections 1 and 2 are related to the ferrofluid velocity in the pipe given by Eq. (8).

$$v_{ci} = \beta_{ci} \frac{dh_p}{dt}, \ \beta_{ci} = \frac{A_p}{A_{ci}}, \ \text{for } i = 1, 2 \tag{8}$$

Substituting Eqs. (3) to (5) in Eq. (2), re-writing all time-dependent variables in terms of $h_p(t)$ using Eq. (6)–(8), and grouping terms results in the one-dimensional equation of motion for ferrofluid rise in the pipe, $h_p(t)$, given by Eq. (9).

$$\begin{aligned} &\mu_0 A_p \int_{h=h_A}^{h=h_I+h_p(t)} \bar{M}(H) \frac{dH(h)}{dh} dh \ - \ \rho A_p g h_p(t) (sin\ \theta + \alpha) \\ &-8\pi\mu \frac{dh_p(t)}{dt} \left[h_p(t) \ + \ l_{c1}\beta_{c1} \ + \ l_{c2}\beta_{c2} \ + \ \alpha \left[h_r(0) - \alpha h_p(t)\right]\right] = \\ &\frac{d^2 h_p(t)}{dt^2} \left[\rho \ A_{c1} l_{c1} \beta_{c1} \ + \ \rho A_{c2} l_{c2} \beta_{c2} \ - \ \rho \ A_r \alpha \left[h_r(0) - \alpha h_p(t)\right] \right. \\ &\qquad \left. + \ \rho A_p h_p(t)\right] \\ &\qquad + \left[\frac{dh_p(t)}{dt}\right]^2 \left[\rho A_p + \rho A_r \alpha^2\right] \end{aligned} \tag{9}$$

The equation of motion being second-order in time, requires two initial conditions for its solution. As noted earlier, the ferrofluid height ($h_p(t)$) is measured relative to its initial level in the reservoir, $h_r(t = 0)$. Therefore the ferrofluid has zero initial displacement given by Eq. (10).

$$h_p(t = 0) = 0 \tag{10}$$

The ferrofluid is always at rest before the electromagnet is powered on. Therefore it has zero initial velocity as given by Eq. (11).

$$\left(\frac{dh_p}{dt}\right)_{t=0} = 0 \tag{11}$$

4. Results

To understand the behaviour of the magnetic pumping, the dynamics of the ferrofluid rise in a vertical pipe as shown in Fig. 4 is considered first. The experimental results are compared against the one-dimensional model. The model is then used to calculate the ferrofluid rise in an inclined pipe. Based on this, the performance of magnetic pumping is calculated and compared against the experimental results.

4.1. Height rise in a vertical pipe

Consider the vertical pipe to be fully filled with the ferrofluid, and the electromagnet is powered on. Recall from Section 2.1 that when a ferrofluid of magnetization $\bar{\mathbf{M}}$ is placed in a magnetic field gradient $\nabla\mathbf{H}$, it experiences a magnetic body force as given by Eq. (1).

When the electromagnet is powered on, an inward acting magnetic body force will act on either end of the electromagnet due to the presence of the magnetic field gradient in that region. Fig. 5 shows the field distribution at the bottom half of the electromagnetic coil. The magnetic force acting on the ferrofluid as a function of its level at the bottom half of the electromagnetic coil is shown in Fig. 6. Here, 0 mm corresponds to the bottom end of the electromagnetic coil. The magnetic force is obtained by varying the limit $h_p(t)$ in Eq. (3), where $\bar{M}(H)$ is obtained from Fig. 3, and $H(h)$ is obtained from Fig. 5. Note that the variation in the magnetic force with axial distance is similar to that of the magnetic field variation shown in Fig. 5, due to their dependence (Eq. (3)). Furthermore, note that the significant force contribution is from the fluid section that experiences the largest gradient which is near the bottom end of the electromagnet. The section of the fluid that is further inside the coil hardly contributes to the overall magnetic force, since the gradient inside the coil is relatively negligible.

Consider that the vertical pipe is partially filled with ferrofluid. The initial ferrofluid level (h_I in Eq. (3)) determines the upward acting magnetic force experienced by it, and thereby its acceleration when the electromagnetic coil is powered on. The initial level of the ferrofluid also determines the time taken to reach the steady state height. This is because when the initial level is relatively low, for example 5 mm in Fig. 6, the upward acting magnetic force will keep increasing as the ferrofluid rises which is opposed by the frictional and gravitational forces. This will take a relatively longer time to reach the steady state height when compared with the scenario where the initial level is higher, for example 40 mm in Fig. 6. In this case, the ferrofluid already experiences most of the upward acting magnetic force when

the electromagnet is powered on. However, a higher starting level also indicates a higher frictional force (Eq. (5)), which could delay the time needed to attain the steady state height. For the magnetic pump discussed in Section 4.3, during each cycle it is desirable that that fluid reaches the end of the rising pipe as quick as possible. This would result in a higher mass flow rate of the pump. However, the mass flow rate is affected by the starting level of the ferrofluid due to the interplay between magnetic and frictional forces discussed above. Therefore there exists an optimum, and based on experiments with different starting levels, a value of 20 mm is chosen for further analysis. At this level, the magnetic force experienced by the ferrofluid when the electromagnet is powered on is 90% of its maximum value (Fig. 6).

When the electromagnetic coil is powered on, the experimentally measured height of the ferrofluid in the vertical pipe as a function of time, $h_p(t)$, is shown in Fig. 7 (thin solid lines) for different maximum magnetic field intensities. Here the shaded regions indicate the measurement errors which include the uncertainties in the displacement sensor reading, as well as in the dimensions of the reservoir and the pipe. The one-dimensional model (Eq. (9)) is numerically solved to obtain $h_p(t)$, and its result is shown in Fig. 7 (thick solid line). It is observed that the simulated values are in reasonable agreement within the errors of the experimentally measured ferrofluid height.

Note that the experimental measurements shows oscillating behaviour after overshoot, while this is not observed in the model. The former is due to the fluid level measurement taken at the reservoir, which is then converted to height variation in the vertical pipe. In the reservoir, as the ferrofluid moves downwards, waves are formed on its surface which results in the observed oscillations, which is not considered in the model.

The maximum magnetic field strength varies from 21.4 mT to 35.7 mT (current of 12 to 20 A respectively). In all these cases it is observed that as the ferrofluid rises, it overshoots. This is attributed to the ferrofluid inertia, a discussion of which is provided below. Following the overshoot it reaches the equilibrium height, which is a balance between the gravitational and the magnetic forces.

The magnetic, gravitational, and frictional forces, along with the net downward force and the net force acting on the ferrofluid with time, as obtained from the model (Eq. (9)) is plotted in Fig. 8. Due to the starting level of the ferrofluid at 20 mm from the electromagnet bottom, it experiences almost 90% of the maximum magnetic force as soon as the electromagnet is powered on, which is at $t = 0$. Thus the magnetic force remains relatively steady when compared with the other forces. The gravitational force (Eq. (4)) scales with the ferrofluid height, and thus its variation with time is qualitatively similar to the variation of the rising fluid with time (Fig. 8).

For a given configuration, the frictional forces (Eq. (5)) mainly varies with the ferrofluid height and its velocity. For comparison, velocity variation with time is also plotted in Fig. 8. The velocity and thereby the viscous forces initially increase with time, reach a maximum, and then reach a minimum before approaching 0 $\mathrm{mm\,s^{-1}}$ and 0 N, respectively. Both these parameters show negative values due to the reversal in the direction of ferrofluid motion following the overshoot.

The net force acting on the ferrofluid is maximum at the start, which causes the velocity to increase steeply with time. This higher acceleration causes a higher frictional force after powering on the electromagnet when compared with the gravitational force. As the ferrofluid level and its velocity increase, so is the net downward force (gravitational + frictional force), and this continues until the magnetic and the net downward forces balance each other. This is seen as the net force on the ferrofluid reaching zero at $t = 0.25$ s, while the velocity and thereby the frictional force is at its maximum i.e. zero acceleration. Note that at this time, the ferrofluid height has reached only about 45% of its equilibrium height.

At $t > 0.25$ s, the net force and thereby the acceleration becomes negative, causing a reduction in the velocity, and frictional forces, while the ferrofluid continues to rise due to inertia.

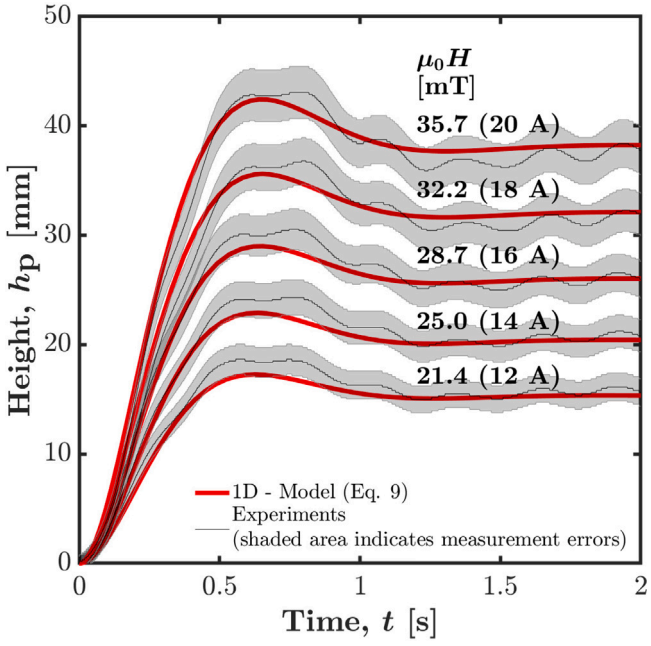

Fig. 7. Dynamics of ferrofluid height rise ($h_p(t)$) in the vertical pipe as a function of time at different maximum applied magnetic fields.

At $t = 0.4$ s, when the net downward force reaches its maximum, the net force reaches its minimum. They occur at the same time because, after $t = 0.3$ s, the magnetic force essentially remains constant, and hence the variation in the net force is a mirror image of the variation in the net downward force.

The ferrofluid first reaches its equilibrium height at $t = 0.48$ s. This can be inferred by observing the gravitational force curve from Fig. 8. For a given magnetic pump configuration, the gravitational force $F_g(t)$ is only dependent on the ferrofluid height in the pipe $h_p(t)$ (Eq. (4)). So the path traced by $F_g(t)$ vs. t curve in Fig. 8 is qualitatively the same as a $h_p(t)$ vs. t curve in Fig. 7. At $t = 0.48$ s, though the velocity is decreasing, it is still positive. Thus the inertial force of the fluid at $t = 0.25$ s, results in an overshoot at $t = 0.48$ s. At the maximum height, while the velocity is zero, the net force is negative. This causes the ferrofluid to change its direction of motion, and finally reach its equilibrium height.

4.2. Height rise in an inclined pipe

To enhance the performance, the ideal design for the magnetic pump would consist of a vertical rising and falling pipe. However, this would cause complexities in bending the electromagnetic coil. Therefore, the rising and falling pipes are inclined. Therefore, the height rise dynamics in the vertical pipe is extended to an inclined pipe. In this case, the major difference is that the flow along the inclined pipe is opposed by a component of the vertical gravitational force. This is accounted for by the $sin\ \theta$ term in Eqs. (4) and (9), where θ is the inclination angle with respect to the horizontal plane. The vertical ferrofluid height in an inclined pipe is given by $h_p(t) sin\ \theta$. The magnetic force acts along the pipe axis, and hence it is not affected by the pipe inclination. To reach the same vertical height, a fluid in an inclined pipe must travel a relatively longer length. This implies that the frictional force increases with pipe inclination for a given vertical height rise. Note that the term $h_p(t)$ in the governing equation (Eq. (9)) denotes the height of the ferrofluid as measured along the pipe axis. So the expression for the frictional force (Eq. (5)) does not have a pipe inclination term in it.

Using the one-dimensional model (Eq. (9)), the variation in the vertical height, i.e. $h_p(t) sin\ \theta$, with time for inclination angles from 10°

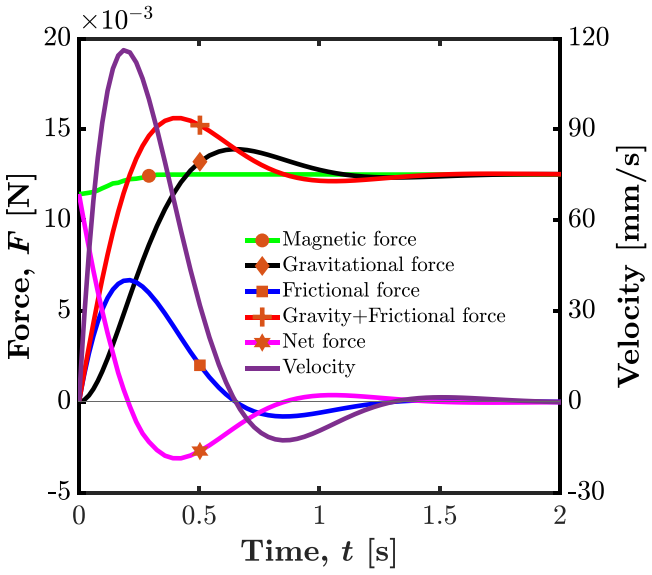

Fig. 8. Variation in different forces and fluid velocity as a function of time, obtained from one-dimensional model (Eq. (9)), for the case $\mu_0 H = 35.7$ mT shown in Fig. 7.

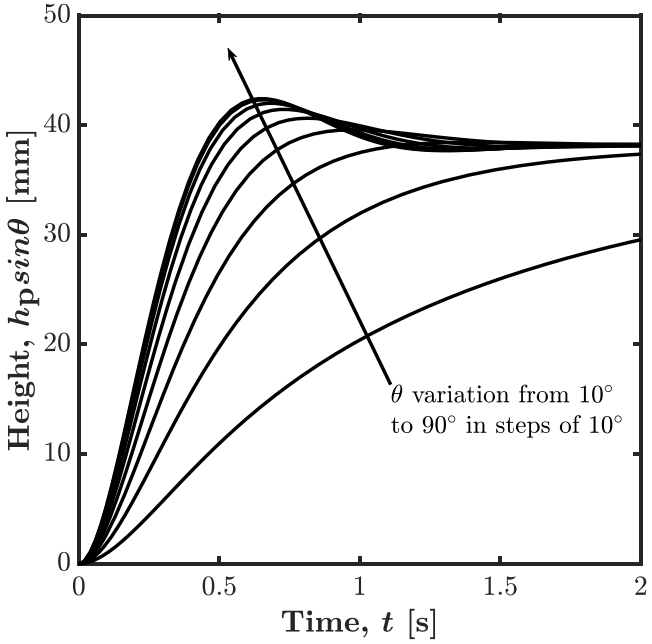

Fig. 9. Vertical ferrofluid height ($h_p(t)sin\theta$), with h_p measured along the pipe axis, as a function of time for pipe inclinations $\theta = 10°$ to 90° with respect to the horizontal ($\mu_0 H = 35.7$ mT.).

to 90° is shown in Fig. 9 for t up to 2 s. In all the cases, the equilibrium vertical height is the same, since the magnetic force is constant in these cases. The difference is that when compared with pipes of higher inclination angles, the fluid has to travel a longer distance along the pipe axis for pipes with lower inclination angles. This means that the time taken to reach the steady state height increases with decreasing inclination angle. Further, it is observed in Fig. 9 that the effect of the overshoot decreases as the inclination angle decreases, and for inclination angles less than 30°, there is no overshoot. This is due to the longer time taken by the ferrofluid to reach the equilibrium height at lower inclination angles. In such scenarios, any inertial force is utilized before the equilibrium height is reached, and thus overshoot is absent.

The height rise dynamics in the inclined pipe is used to model the magnetic pumping behaviour as explained in the following section.

4.3. Magnetic pumping

The working of the magnetic pump was discussed in Section 2. To test its performance, the vertical pipe in Fig. 4 was replaced by an inclined rising and a falling pipe as shown in Figs. 10 and 11(b). The inclinations of the rising and falling pipes are 29.0° and 23.7° with respect to horizontal, respectively. The values of l_{c1} and l_{c2} (refer Fig. 4(a)) is 250 mm and 110 mm respectively. The inner radius of connection pipes 1 and 2 are 5 mm and 3 mm respectively.

The experimentally measured area averaged mass flow rate of the ferrofluid pumped as a function of the magnetic field frequency for pumping height (Δh) of 0 mm to 6 mm is shown in Fig. 11(a). Here Δh is the difference in height between the initial ferrofluid level in the rising pipe and the bottom of the outlet in the falling pipe. When the electromagnet is powered on, the ferrofluid fills the rising and falling pipe, and when it is powered off, the ferrofluid in the falling pipe flows out due to gravity. Thus the pumping action is intermittent. The mass flow rate shown in Fig. 11(a) is time averaged so that it can be compared with the designs that provide continuous pumping.

The present magnetic pump utilizes magnetic body forces due to gradient in magnetic fields for pumping. So the design is scalable across multiple length scales of pipe diameters, for example from millimetres to metres. Therefore, the mass flow rate shown in the left vertical axis of Fig. 11(a), can be divided by cross-sectional area to obtain the area normalized mass flow rate, and is indicated on the right vertical axis. This allows the performance of the developed magnetic pump design to be compared with other designs having different pipe sizes.

It is observed from Fig. 11(a), that for a given pumping height (Δh), there exists an optimal frequency at which the mass flow rate is maximum. At frequencies lower than the optimal value, the time for which the electromagnet is powered on is longer than the time required to fill the falling pipe. Therefore, though the falling pipe is filled, the mass flow rate approaches zero as the frequency decreases. At frequencies higher than the optimal value, the time for which the electromagnet is powered on is not sufficient for the falling pipe to be completely filled. The level of filling in the falling pipe decreases with increasing frequency, and beyond a certain limit, no ferrofluid reaches the falling pipe, thus resulting in zero mass flow rate.

As pumping height (Δh) increases, the fluid will take longer time to reach the falling pipe. Therefore, the optimal frequency will shift towards the lower frequencies as can be seen in Fig. 11(a).

The one-dimensional model for an inclined pipe is used to simulate the magnetic pumping process. For this, an inclined pipe with length $L_r = 140$ mm and angle $\theta_r = 29°$ (Fig. 2) is considered which mimics the rising pipe. The flow behaviour in such an arrangement was discussed in Section 4.2, where the vertical pipe length was higher than the steady state height of the fluid. However, for the case of magnetic pumping process, the vertical pipe length ($L_r \sin\theta$) should be lower than the steady state height reached for a given magnetic field distribution. This is to ensure that the fluid can reach the falling pipe.

For the pumping model, when the fluid reaches the end of the rising pipe, it is assumed that it will instantaneously fall into the falling pipe. However, in reality it would indeed take a finite time, and depending on the velocity and pipe geometry, the fluid at the end of the rising pipe could also experience resistance. The implication of ignoring such effects is that, when the electromagnet is powered on, the mass of the fluid filled in the falling pipe could be higher than the experimentally measured value. Of $L_r = 140$ mm considered, 110 mm was the actual length of the rising pipe, while the additional 30 mm is added to account for the additional resistance encountered. This value was determined by comparing the experimental and simulated values for a single value of pumping height. When the electromagnet is powered off, in reality the fluid will take a finite time to empty

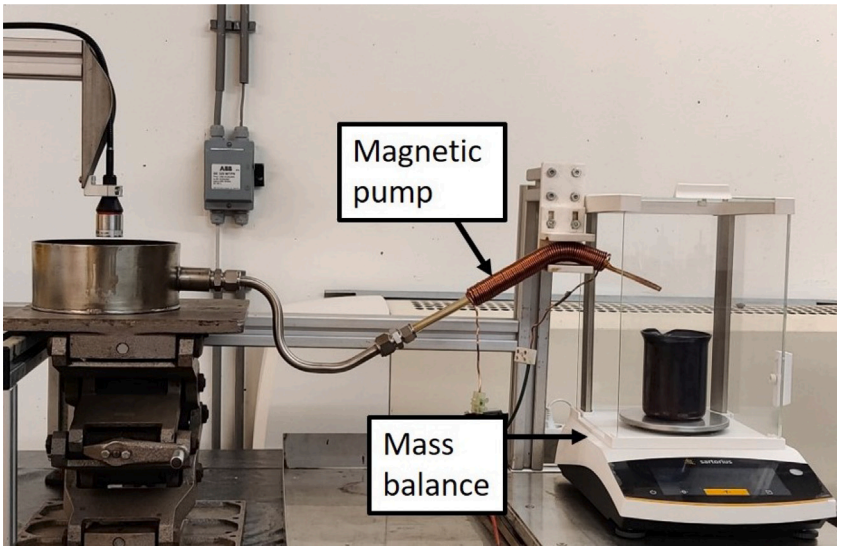

Fig. 10. Experimental setup for testing the magnetic pump performance.

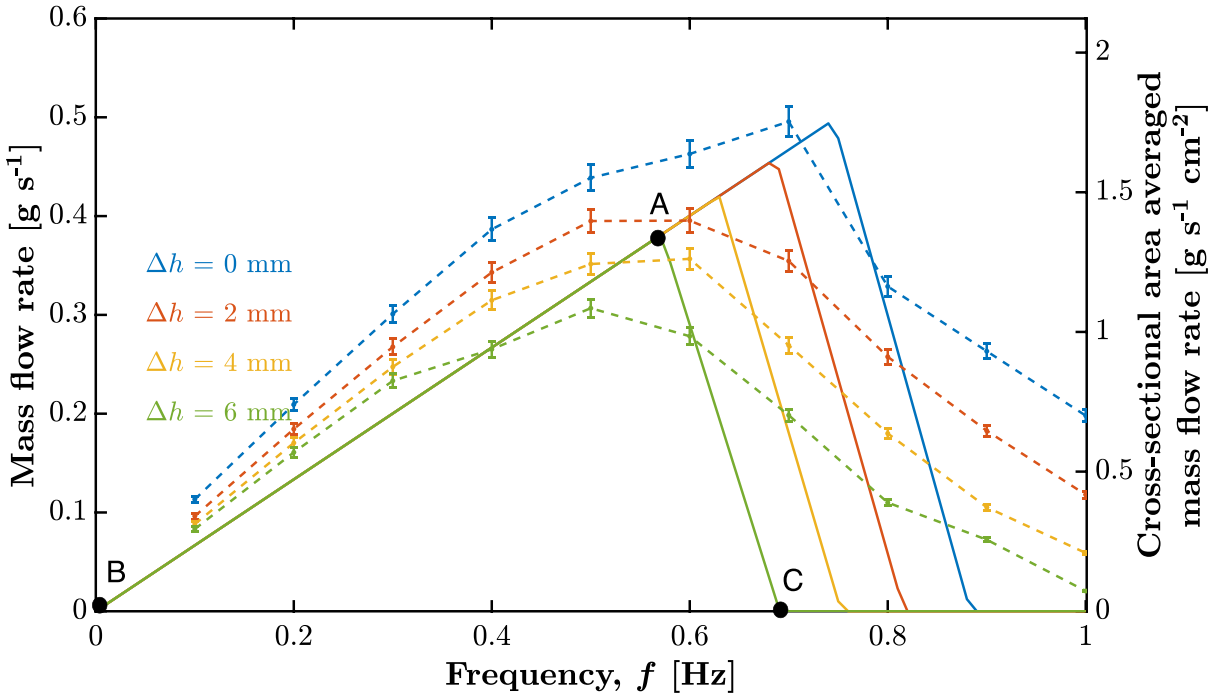

(a)

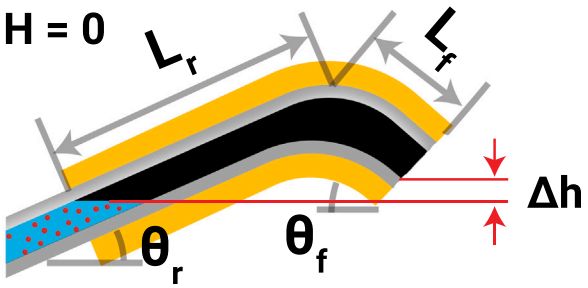

(b)

Fig. 11. (a) Mass flow rate of ferrofluid pumped as a function of magnetic field frequency for different pumping heights at $\mu_0 H = 35.7$ mT. The dotted line represents experimentally measured values, while the continuous line represents values obtained from one-dimensional model. (b) Illustration indicating the measurement of Δh.

from the falling pipe. The time for which the electromagnet is powered on and off is of the same duration, i.e. the magnetic field pulse is symmetric. For the geometry and angle of the magnetic pump used in experimental characterization, it was observed that the time taken to empty the falling pipe during each magnetic field pulse in continuous operation, is less than the off time of the electromagnet. Therefore, in the magnetic pumping simulation, it is considered that the fluid in the falling pipe would be emptied completely during the off time of the magnetic field pulse for a given frequency. As frequency increases, the off time reduces and the fluid in the falling pipe may not have sufficient time for outflow. However beyond a certain frequency, it should be noted that there will be no fluid reaching the falling pipe.

The results of the simulated magnetic pumping behaviour is shown in Fig. 11(a) along with the experimental results with error bars. It is seen that quantitatively there is a considerable disagreement between the frequency and the mass flow rate. However, qualitatively a similar trend is observed. This indicates that, usage of a higher dimensional model is required to better predict the magnetic pumping process.

A performance curve such as the one for $\Delta h = 6$ mm in Fig. 11(a) has among others, three typical points of interest — marked as A, B, and C. Of these, point A is at the maximum mass flow rate. The other two points – B and C, correspond to points of zero mass flow rate on either side of point A. The mass flow rate dependence on time (and hence on frequency) at these points can be expressed as:

$$\dot{m} = \frac{m}{t_{\text{on}} + t_{\text{off}}} \quad \text{where} \quad m \begin{cases} = m_{max} & \text{if } t_{\text{on}} \geq t_{\max} \\ \propto (t_{\text{on}} - t_{\text{r}}) & \text{if } t_{\text{r}} < t_{\text{on}} < t_{\max} \\ = 0 & \text{if } t_{\text{on}} \leq t_{\text{r}} \end{cases} \tag{12}$$

In the above equation, $\dot{m}$ is the mass flow rate pumped [$\mathrm{g\,s^{-1}}$], m is the fluid mass collected in the falling pipe during a cycle [g], t_{on} and t_{off} corresponds to the time for which the electromagnet is powered on and off respectively [s], $t_{\max}$ is the time for which the electromagnet is to be on when the fluid completely fills the falling pipe [s]. The corresponding fluid mass in the falling pipe is m_{max} [g]. The electromagnet is operated at a symmetric cycle, i.e. $t_{\text{on}} = t_{\text{off}}$. Therefore, the time corresponding to point A is twice that of $t_{\max}$, i.e. $t_{\text{A}} = 2t_{\max} = 1/f_{\text{A}}$. For a given magnetic pump configuration, let t_{r} represents the time required for the ferrofluid to rise in the rising pipe such that it is just about to enter the falling pipe. Then point C corresponds to the scenario when the electromagnet is powered on for $t_{\text{on}} = t_{\text{r}}$. Therefore, $t_{\text{C}} = 2t_{\text{r}} = 1/f_{\text{C}}$. Point B corresponds to an infinitely long cycle time, i.e. $f_{\text{B}} = 0$ Hz.

It is seen from Eq. (12) that the two important time parameters are $t_{\max}$ and t_{r}. These two times are proportional to the volume of rising (V_{r}) and falling pipe (V_{f}). These are related to the geometric parameters as shown in Eqs. (13) and (14).

$$t_{\text{r}} \propto V_{\text{r}} \propto L_{\text{r}}\, \theta_{\text{r}}\, \Phi_{\text{r}} \tag{13}$$

$$t_{\max} \propto V_{\text{f}} \propto L_{\text{f}}\, \theta_{\text{f}}\, \Phi_{\text{f}} \tag{14}$$

where L, θ and Φ are the length, inclination, and inner diameter of the rising (subscript r) and falling (subscript f) pipe respectively.

The six geometrical parameters in Eqs. (13) and (14) determine the position of points A and C. These in turn determine the slopes of the two lines BA and AC (Fig. 11(a)). The ratio of these two slopes (λ) is given by eq, (15).

$$\lambda = \frac{\text{Slope BA}}{\text{Slope AC}} = 1 - \frac{t_{\text{A}}}{t_{\text{C}}} \tag{15}$$

Due to the position of A and C, $t_{\text{A}} > t_{\text{C}}$. This means that λ would always be negative, as expected. For the case $\Delta h = 6$ mm in Fig. 11(a) the magnitude of slope AC is nearly six times higher than that of BA. The slopes would have equal magnitude when $t_{\text{A}} = 2t_{\text{C}}$.

For $\Delta h = 0$ mm, it is observed from Fig. 11(a) that a cross-sectional area averaged mass flow rate of around 1.8 $\mathrm{g\,s^{-1}\,cm^{-2}}$ is obtained for $\mu_0 H = 35.7$ mT and 0.74 Hz. This flow rate is comparable to the flow rates reported by the magnetic pumps based on travelling wave magnetic fields when averaged for applied magnetic field [45]. However, for such pumps the optimal frequency is in the range of 1000 Hz, whereas for the presently developed pump it is less than 1 Hz. Such low operational frequencies are desirable in applications such as a magnetocaloric mixture based refrigerator where higher operational frequencies could lead to detrimental heating effects. Apart from frequency, the efficiency of pumping (ξ) is also an important parameter. It is given by the ratio of fluid flow power to input power (Eq. (16)).

$$\xi = \frac{\dot{m}\ \Delta P}{1000 * \rho\ V I} \tag{16}$$

where $\dot{m}$ is mass flow rate pumped [$\mathrm{g\,s^{-1}}$], ΔP is the pressure drop encountered by the fluid flow [$\mathrm{N\,m^{-2}}$], V and I are the voltage [V] and the current [A] supplied to the electromagnet, respectively. The term "VI" represents the electrical power supplied to the electromagnet.

The discussion of ferrohydrodynamic pumping efficiency is limited in the literature, and nearly no experimentally measured values are available. One reason for this could be the nature of applications where achieving a fluid flow is more important than its efficiency.

For all the operating conditions shows in Fig. 11(a), the measured efficiency of the tested magnetic pump is less than 1%. A main advantage of magnetic refrigeration is its increased energy efficiency when compared to vapour compression refrigeration technology. To maintain this advantage, it is necessary that the components used in magnetic refrigeration are best in their category. Mechanical pumps typically have efficiencies of 50% or higher. The present magnetic pump is an initial step, and future work aiming to increase its efficiency, for example by innovative design with iron core, is necessary for its adoption in magnetic refrigeration.

5. Conclusions

A design for a magnetic pump that works with low magnetic field frequencies (<1 Hz) is proposed with its performance experimentally characterized and compared against a one-dimensional model.

The design of the magnetic pump consists of a rising and falling pipe, enclosed by an electromagnetic coil. On application of magnetic field, due to the inward acting force on either end of the pipes, the ferrofluid progresses in the rising pipe and reaches the falling pipe. On removal of the magnetic field, the portion of the fluid in the falling pipe falls down due to gravity, thereby achieving a net pumping action. Thus on continuously cycling the magnetic field, an intermittent motion of the ferrofluid is obtained. Care is taken to ensure that syphoning phenomena did not occur. The maximum cross-sectional area averaged mass flow rate of the proposed design is around 1.8 $\mathrm{g\,s^{-1}\,cm^{-2}}$ at 0.74 Hz and 35.7 mT. This mass flow rate is comparable to pump designs that utilizes travelling wave magnetic fields, whose optimal frequency is three orders of magnitude higher. Such low frequency operation of the developed pump can be used in applications where heating effects that result from high frequencies would be detrimental to the system performance.

In order to understand the dynamics of the pump, initially the dynamics of the height rise in a vertical pipe was studied for different magnetic field strengths. For the configuration tested, in each case the fluid overshoots before achieving a steady state height, where the magnetic and gravitational forces are in equilibrium. This process is simulated using a one-dimensional fluid flow model, and its results match reasonably well with the experiments. The model is then used to obtain the height rise dynamics of the inclined pipe. This is used to model the behaviour of the magnetic pump, whose results agree qualitatively with the experimental results. A considerable quantitative difference exists. This suggests the presence of other effects that occur during magnetic pumping, and implies the need for usage of higher dimensional model for simulations. Further work on the efficiency improvement of the developed pump is necessary for its adoption in a magnetic refrigerator with no moving parts.

Nomenclature

Symbol	Description	Unit
A_{c1}, A_{c2}	Cross-sectional area of connecting section c1 and c2.	[m^2]
A_p	Pipe cross-sectional srea	[m^2]
A_r	Reservoir cross-sectional srea	[m^2]
F_g	Gravitational force	[N]
F_f	Frictional force	[N]
F_M	Magnetic force	[N]
$\boldsymbol{F}_{MBF}$	Magnetic body force	[N m^{-3}]
g	Acceleration due to gravity	[m s^{-2}]
h_A	Position below the electromagnet where magnetic field is zero	[m]
h_I	Ferrofluid initial level measured relative to h_A	[m]
h_p	Ferrofluid height in pipe	[m]
h_r	Ferrofluid height in reservoir	[m]
$h_{r\text{-}c}$	Reduction in the ferrofluid height at the reservoir when compared to $h_r(t=0)$	[m]
H	Applied magnetic field	[A m^{-1}]
I	Current	[A]
l_{c1}, l_{c2}	Length of connecting section c1 and c2.	[m]
L	Rising/falling pipe length	[m]
m	Fluid mass collected in falling pipe during a cycle	[g]
$\dot{m}$	Mass flow rate pumped	[g s^{-1}]
m_{max}	Fluid mass corresponding to t_{max}	[g]
$\bar{M}$	Magnetization of the particle	[A m^{-1}]
ΔP	Pressure drop	[N m^{-2}]
t	Time	[s]
t_{on}, t_{off}	Time for which the electromagnet is powered on and off respectively	[s]
t_{max}	Time for which the electromagnet is to be on when the fluid completely fills the falling pipe	[s]
t_r	Time required for the ferrofluid to rise	[s]
v_{c1}, v_{c2}	Ferrofluic velocity in connecting section c1 and c2.	[m s^{-1}]
V	Voltage	[V]
V_r, V_f	Volume of rising and falling pipe	[m^3]
μ_0	Magnetic permeability of vacuum	[kg m s^{-2} A^{-2}]
θ	Inclination angle of the pipe with respect to the horizontal	[°]
Φ	Rising/falling pipe inner diameter	[m]
ρ	Density of ferrofluid	[kg m^{-3}]
μ	Dynamic viscosity of ferrofluid	[kg m^{-1} s^{-1}]

CRediT authorship contribution statement

Keerthivasan Rajamani: Writing – review & editing, Writing – original draft, Methodology, Investigation, Formal analysis, Data curation, Conceptualization. **Eva Juffermans:** Methodology, Investigation, Data curation. **Luca Granelli:** Investigation, Formal analysis, Data curation. **Ana De Cuadra Rabaneda:** Formal analysis, Data curation. **Wilko Rohlfs:** Investigation. **Marcel ter Brake:** Writing – review & editing, Supervision, Methodology, Investigation, Formal analysis. **Theo van der Meer:** Writing – review & editing, Supervision, Investigation, Formal analysis. **Mina Shahi:** Writing – review & editing, Supervision, Project administration, Methodology, Investigation, Funding acquisition, Formal analysis, Conceptualization.

Declaration of competing interest

The authors declare the following financial interests/personal relationships which may be considered as potential competing interests: Keerthivasan Rajamani, Theo van der Meer, Marcel ter Brake, and Mina Shahi has filed for patent for the magnetic pump at the European Patent Office pending to the University of Twente.

Data availability

Data will be made available on request.

Acknowledgments

The present work is part of the research programme NETMNF with project number 15401, which is (partly) financed by the Netherlands Organization for Scientific Research (NWO).

References

[1] Brown JS, Domanski PA. Review of alternative cooling technologies. Applied Thermal Engineering 2014;64(1-2):252–62.
[2] Kitanovski A. Energy applications of magnetocaloric materials. Adv Energy Mater 2020;10(10):1903741.
[3] Zimm C, Jastrab A, Sternberg A, Pecharsky V, Gschneidner K, Osborne M, Anderson I. Description and performance of a near-room temperature magnetic refrigerator. In: Advances in cryogenic engineering. Springer; 1998, p. 1759–66.
[4] Gschneidner KA, Pecharsky VK. Thirty years of near room temperature magnetic cooling: Where we are today and future prospects. Int J Refrig 2008;31(6):945–61.
[5] Brück E. Developments in magnetocaloric refrigeration. J Phys D: Appl Phys 2005;38(23):R381.
[6] Brück E. Chapter four magnetocaloric refrigeration at ambient temperature. Handb Magn Mater 2007;17:235–91.
[7] Weiss P, Piccard A. Le phénomène magnétocalorique. J Phys Theor Appl 1917;7(1):103–9.
[8] Smith A. Who discovered the magnetocaloric effect? Eur Phys J H 2013;38(4):507–17.
[9] Tishin AM, Spichkin YI. The magnetocaloric effect and its applications. CRC Press; 2016.
[10] Pecharsky V, Gschneidner Jr. K, Pecharsky A, Tishin A. Thermodynamics of the magnetocaloric effect. Phys Rev B 2001;64(14):144406.
[11] Pecharsky VK, Gschneidner Jr. KA. Magnetocaloric effect and magnetic refrigeration. J Magn Magn Mater 1999;200(1–3):44–56.
[12] Zimm C, Boeder A, Mueller B, Rule K, Russek SL. The evolution of magnetocaloric heat-pump devices. MRS Bull 2018;43(4):274–9.
[13] Debye P. Einige bemerkungen zur magnetisierung bei tiefer temperatur. Ann Phys 1926;386(25):1154–60.
[14] Giauque W. A thermodynamic treatment of certain magnetic effects. a proposed method of producing temperatures considerably below 1 absolute. J Am Chem Soc 1927;49(8):1864–70.
[15] Giauque W, MacDougall D. Attainment of temperatures below 1° absolute by demagnetization of $Gd_2(SO_4)_3 \cdot 8H_2o$. Phys Rev 1933;43(9):768.
[16] Brown GV. Magnetic heat pumping near room temperature. J Appl Phys 1976;47(8):3673–80.
[17] Yuan L, Qian S, Yu J. Numerical study on the multi-layered magnetocaloric regenerators. Appl Therm Eng 2022;204:118001.
[18] Teyber R, Trevizoli P, Christiaanse T, Govindappa P, Niknia I, Rowe A. Performance evaluation of two-layer active magnetic regenerators with second-order magnetocaloric materials. Appl Therm Eng 2016;106:405–14.
[19] Masche M, Liang J, Engelbrecht K, Bahl C. Performance assessment of a rotary active magnetic regenerator prototype using gadolinium. Appl Therm Eng 2022;204:117947.
[20] Kitanovski A, Tušek J, Tomc U, Plaznik U, Ozbolt M, Poredoš A. Magnetocaloric energy conversion: From theory to applications. Green Energy and Technology, Springer International Publishing; 2015.
[21] Rosensweig RE. Ferrohydrodynamics. Courier Corporation; 2013.
[22] Odenbach S. Ferrofluids: Magnetically controllable fluids and their applications. vol. 594, Springer; 2008.

[23] Alexiou C, Arnold W, Klein RJ, Parak FG, Hulin P, Bergemann C, Erhardt W, Wagenpfeil S, Lubbe AS. Locoregional cancer treatment with magnetic drug targeting. Cancer Res 2000;60(23):6641–8.
[24] Jurgons R, Seliger C, Hilpert A, Trahms L, Odenbach S, Alexiou C. Drug loaded magnetic nanoparticles for cancer therapy. J Phys: Condens Matter 2006;18(38):S2893.
[25] Bailey R. Lesser known applications of ferrofluids. Journal of magnetism and magnetic materials 1983;39(1-2):178–82.
[26] Kole M, Khandekar S. Engineering applications of ferrofluids: a review. Journal of Magnetism and Magnetic Materials 2021;537:168222.
[27] Raj K, Moskowitz R. A review of damping applications of ferrofluids. IEEE Transactions on Magnetics 1980;16(2):358–63.
[28] Al-Habahbeh O, Al-Saqqa M, Safi M, Khater TA. Review of magnetohydrodynamic pump applications. Alex Eng J 2016;55(2):1347–58.
[29] Homsy A, Koster S, Eijkel JC, van den Berg A, Lucklum F, Verpoorte E, de Rooij NF. A high current density DC magnetohydrodynamic (MHD) micropump. Lab Chip 2005;5(4):466–71.
[30] Dunne P, Adachi T, Dev AA, Sorrenti A, Giacchetti L, Bonnin A, Bourdon C, Mangin PH, Coey J, Doudin B, et al. Liquid flow and control without solid walls. Nature 2020;581(7806):58–62.
[31] Hatch A, Kamholz AE, Holman G, Yager P, Bohringer KF. A ferrofluidic magnetic micropump. J Microelectromech Syst 2001;10(2):215–21.
[32] Matia Y, An HS, Shepherd RF, Lazarus N. Magnetohydrodynamic levitation for high-performance flexible pumps. Proc Natl Acad Sci 2022;119(29):e2203116119.
[33] Cao X, Xuan S, Hu T, Gong X. 3D printing-assistant method for magneto-active pulse pump: Experiment, simulation, and deformation theory. Appl Phys Lett 2020;117(24):241901.
[34] Fuhrer R, Schumacher CM, Zeltner M, Stark WJ. Soft iron/silicon composite tubes for magnetic peristaltic pumping: frequency-dependent pressure and volume flow. Adv Funct Mater 2013;23(31):3845–9.
[35] Tang S-Y, Zhang X, Sun S, Yuan D, Zhao Q, Yan S, Deng L, Yun G, Zhang J, Zhang S, et al. Versatile microfluidic platforms enabled by novel magnetorheological elastomer microactuators. Adv Funct Mater 2018;28(8):1705484.
[36] Liu JF, Yadavali S, Tsourkas A, Issadore D. Microfluidic diafiltration-on-chip using an integrated magnetic peristaltic micropump. Lab Chip 2017;17(22):3796–803.
[37] Finlayson B. Convective instability of ferromagnetic fluids. J Fluid Mech 1970;40(4):753–67.
[38] Neuringer JL, Rosensweig RE. Ferrohydrodynamics. Phys Fluids 1964;7(12):1927–37.
[39] Pattanaik M, Varma V, Cheekati S, Chaudhary V, Ramanujan R. Optimal ferrofluids for magnetic cooling devices. Sci Rep 2021;11(1):1–19.
[40] Moskowitz R, Rosensweig R. Nonmechanical torque-driven flow of a ferromagnetic fluid by an electromagnetic field. Appl Phys Lett 1967;11(10):301–3.
[41] Zahn M. Ferrohydrodynamic torque-driven flows. J Magn Magn Mater 1990;85(1–3):181–6.
[42] Zahn M, Wainman PN. Effects of fluid convection and particle spin on ferrohydrodynamic pumping in traveling wave magnetic fields. J Magn Magn Mater 1993;122(1–3):323–8.
[43] Zahn M, Greer DR. Ferrohydrodynamic pumping in spatially uniform sinusoidally time-varying magnetic fields. J Magn Magn Mater 1995;149(1–2):165–73.
[44] Mao L, Koser H. Ferrohydrodynamic pumping in spatially traveling sinusoidally time-varying magnetic fields. J Magn Magn Mater 2005;289:199–202, Proceedings of the 10th International Conference on Magnetic Fluids.
[45] Mao L, Elborai S, He X, Zahn M, Koser H. Direct observation of closed-loop ferrohydrodynamic pumping under traveling magnetic fields. Phys Rev B 2011;84(10):104431.
[46] Mao L, Koser H. Towards ferrofluidics for μ-TAS and lab on-a-chip applications. Nanotechnology 2006;17(4):S34.
[47] EFH Series Ferrofluid - Safety Data Sheet, https://ferrofluid.ferrotec.com/wp-content/uploads/sites/3/efhsds.pdf accessed: 02-10-2023.